

Safe Control of Quadruped in Varying Dynamics via Safety Index Adaptation

Kai S. Yun¹, Rui Chen², Chase Dunaway³, John M. Dolan², Changliu Liu²

Abstract—Varying dynamics pose a fundamental difficulty when deploying safe control laws in the real world. Safety Index Synthesis (SIS) deeply relies on the system dynamics and once the dynamics change, the previously synthesized safety index becomes invalid. In this work, we show the real-time efficacy of Safety Index Adaptation (SIA) in varying dynamics. SIA enables real-time adaptation to the changing dynamics so that the adapted safe control law can still guarantee 1) forward invariance within a safe region and 2) finite time convergence to that safe region. This work employs SIA on a package-carrying quadruped robot, where the payload weight changes in real-time. SIA updates the safety index when the dynamics change, e.g., a change in payload weight, so that the quadruped can avoid obstacles while achieving its performance objectives. Numerical study provides theoretical guarantees for SIA and a series of hardware experiments demonstrate the effectiveness of SIA in real-world deployment in avoiding obstacles under varying dynamics.

I. INTRODUCTION

In this work, we study the safe control of quadruped robots in a realistic scenario: carrying objects of varying weights. Quadrupeds have been studied for real-world tasks such as helping the visually-impaired [1], towing objects collaboratively [2], and even performing parkour stunts [3]. When deploying robots in real-world settings [4, 5, 6, 7, 8], it is essential to ensure safety. In particular, safety guarantees under varying dynamics are of paramount interest. For a shopping companion quadruped, the payload on its back will constantly change as the human loads it with different products. Under such changing dynamics, how can the quadruped maintain safety, i.e., avoid collisions? This is the exact question that this work addresses.

We achieve this by using safety index adaptation (SIA) [9]. SIA allows safe control laws to adapt to changing dynamics within seconds, mitigating safety risks from dynamic mismatches. SIA is a member of the safe set algorithm (SSA) family [10], a widely studied method to ensure constraint satisfaction for dynamic systems. SSA quantifies safety using energy functions and derives safe control laws that keep the system states within a user-specified safe region, ensuring forward invariance (FI), meaning the system stays in the safe region once entered [11]. While this is sufficient for safety guarantees when the system starts in a safe state, practical issues such as discretization errors and hardware

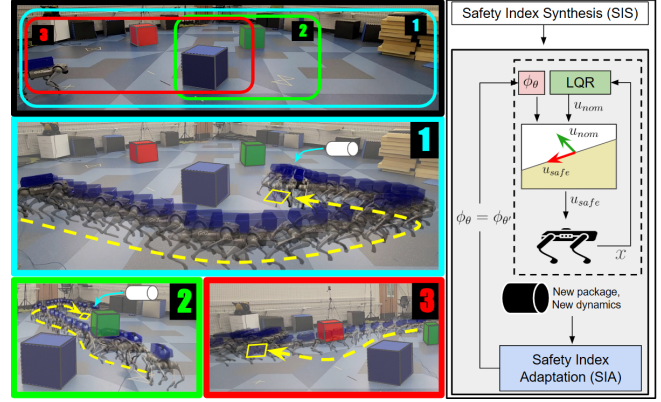


Fig. 1. Trajectory of the quadruped carrying various packages of different weights (left column) and overall pipeline (right column). The quadruped avoids each obstacle sequentially, in the order of (1) blue, (2) green, and (3) red cubes, using safety index. Once the quadruped arrives at a goal position after avoiding an obstacle, a different package is loaded on its back. At this point, the safety index is adapted to the new dynamics.

noise may cause the system to drift into unsafe regions when the robot operates near the safe region boundary. To address this, the control law must also ensure finite-time convergence (FTC), bringing the system back to safety [11]. Although safety index synthesis (SIS) [11, 12] provides a systematic method of constructing feasible and safe control laws, it does not provide such guarantees when the dynamics change. Reapplying SIS for each new dynamics is impractical, as it can take several minutes, even for simple dynamics. To handle this, safety index adaptation (SIA) [9] has been proposed.

Here, we test SIA on physical robots for the first time and demonstrate the effectiveness of SIA in changing real-world dynamics. Specifically, we apply SIA to a quadruped robot tasked with navigating multiple goals while carrying varying payloads and avoiding obstacles. We demonstrate that SIA is essential to avoid safety failures under varying dynamics and fast enough for online adaptation. To summarize, our contributions are:

- We guarantee safety for real quadruped robots in navigation tasks with varying dynamics.
- We improve the efficiency of safety index adaptation and validate its efficacy in real life.
- We provide a comprehensive analysis of the safety characteristics of adapted safety indices.
- We introduce a linear model for the varying quadruped dynamics and a method to identify varying parameters.

¹Mechanical Engineering Department, Carnegie Mellon University, Pittsburgh, PA. Contact: sirkhooy@andrew.cmu.edu

²Robotics Institute, Carnegie Mellon University, Pittsburgh, PA. Contact: {rui3, jdolan, cliu6}@andrew.cmu.edu

³Mechanical Engineering Department, New Mexico Institute of Mining and Technology, Socorro, NM. Contact: chase.dunaway@student.nmt.edu

II. RELATED WORK

Formal SIS uses sum-of-squares programming (SOSP) to construct feasible and safe control laws. [12] tackles SIS for known systems with control bounds, while [11] extends this to state-dependent control bounds. Another line of work in safe control is control barrier functions (CBF) [13, 14], which also uses energy functions to quantify safety. While SIS is a subset of CBF synthesis [15, 16, 17, 18, 19], SIS targets a specific class of energy functions usually for collision avoidance and considers both FI and FTC.

As previously mentioned, real-world dynamics are imperfectly known and usually change over time. [20, 21] propose robust CBFs (rCBFs) to provide safety under bounded uncertainties, while [22] develops adaptive CBFs (aCBFs) to estimate the changes in the dynamics. Although safe controller synthesis for constant dynamics has been studied extensively, synthesis of adaptive safe controllers under changing dynamics has not been studied widely to our knowledge. [23] uses SOSP to synthesize a robust-adaptive CBF (raCBF) that applies adaptive safe control for systems with bounded parametric uncertainties. [24, 25] assume bounded dynamics noise for its aCBF, but lack the mathematical rigor required for safety guarantees since they use learning-based methods. [9] leverages Sylvester's criterion to readily adapt safety index to varying dynamics while guaranteeing safety constraints. It provides the central theory and methodology for our work, but has only been tested in simulation for a 2-DOF robot. For safe control of quadruped hardware, [6] uses Hamilton-Jacobi-based safeguard for agile locomotion, but does not provide safety guarantees. While [26] uses CBF for rough terrain locomotion and [27] utilizes CBF to walk through narrow spaces, these do not consider varying dynamics. This paper addresses the growing interest in providing *adaptive safety assurance for quadrupeds*.

III. PRELIMINARIES

A. Safe Control for Varying Dynamics

The system state is $x \in \mathcal{X} \subseteq \mathbb{R}^{N_x}$ and the control input is $u \in \mathcal{U} \subseteq \mathbb{R}^{N_u}$. The state-space \mathcal{X} is bounded with inequalities, i.e., $\mathcal{X} = \{x : h_i(x) \geq 0, \forall i = 1, \dots, N_h\}$ and the control space \mathcal{U} is bounded element-wise, i.e., $\mathcal{U} = \{u : \underline{u} \leq u \leq \bar{u}\}$. The nominal dynamics, without concern for the changes in dynamics is $\dot{x}_{nom} = f(x) + g(x)u$, $u \in \mathcal{U}$ with $f : \mathbb{R}^{N_x} \rightarrow \mathbb{R}^{N_x}$ and $g : \mathbb{R}^{N_x} \rightarrow \mathbb{R}^{N_x \times N_u}$, both locally Lipschitz continuous. In practice, system dynamics are usually varying, and it is critical to parameterize the changing dynamics and incorporate their changes with the safe control law. To this end, we denote the varying parameters as ρ and extend the nominal dynamics, following [9]. In this work, we consider the following parameter-varying dynamics:

$$\dot{x} = f(x, \rho) + g(x, \rho)u = A^f f(x) + A^g g(x)u + \epsilon, \quad (1)$$

where $A^f := \text{diag}([\rho_{11}^f, \rho_{22}^f, \dots, \rho_{N_x N_x}^f])$ is a real diagonal matrix, $A^g \in \mathbb{R}^{N_x \times N_x}$ is a free-form real matrix, and $\epsilon = [\rho_1^\epsilon, \rho_2^\epsilon, \dots, \rho_{N_x}^\epsilon]^T$ is a real vector.

We enforce safety with two objectives [11]: (C.1) *forward invariance (FI)* and (C.2) *finite-time convergence (FTC)*. Given a user-specified *safety specification*, defined with a piecewise-smooth function $\phi_0(x) : \mathcal{X} \rightarrow \mathbb{R}$, forward invariance means that if the state x is already within the *forward invariant set*, \mathcal{X}_S^* , which is a subset of the *safe set*, $\mathcal{X}_S = \{x : \phi_0(x) \leq 0\}$, it should never leave that set. Finite-time convergence means that if the state x is outside the forward invariant set, it should land in that set in finite time.

Safe set algorithm (SSA) [10] provides a method for designing a general n^{th} ($n \geq 0$) order, linearly parameterized *safety index* ϕ_n that can handle general relative degrees (> 1) between ϕ_0 and the control input u . $\phi_n : \mathcal{X} \rightarrow \mathbb{R}$, is a continuous, piecewise-smooth energy function that measures safety and defines forward invariant set $\mathcal{X}_S^* = \{x : \phi_n(x) \leq 0\}$. It is designed as $\phi_n = [\prod_{i=1}^n (1 + a_i s)] \phi_0$, where s is the differentiation operator. This can be expanded to

$$\phi_n := \phi_0 + \sum_{i=1}^n k_i \phi_0^{(i)} \quad (2)$$

where $\phi_0^{(i)}$ is the i^{th} time derivative of ϕ_0 . SSA uses the following optimization as the safe control law:

$$\min_{u \in \mathcal{U}} \mathcal{J}(u) \quad \text{s.t.} \quad \dot{\phi}_\theta(x, u) < -\eta \text{ if } \phi_\theta(x) \geq 0 \quad (3)$$

where the objective \mathcal{J} is arbitrary. [9, 11] show that if the following conditions are satisfied, both FI and FTC are guaranteed: (i) the characteristic equation $\prod_{i=1}^n (1 + a_i s) = 0$ only has negative real roots, (ii) the relative degree from $\phi_0^{(n)}$ to control input is one, and (iii) there always exists a control u that satisfies (3). The conditions (i) and (ii) above are easy to hold by design, while (iii) is non-trivial to satisfy. In the next subsection, we summarize how (iii) is achieved via safety index synthesis.

B. Safety Index Synthesis

Designing a safety index that achieves the safety guarantees involves choosing the right parameterization for (2). This process is referred to as *Safety Index Synthesis (SIS)*:

Problem 1. (Safety Index Synthesis). *Find safety index as $\phi_\theta := \phi_0 + \sum_{i=1}^n k_i \phi_0^{(i)}$ with parameter $\theta \in \Theta := \{[k_1, k_2, \dots, k_n] : k_i \in \mathbb{R}, k_i \geq 0, \forall i\}$, such that*

$$\forall x \in \mathcal{X} \quad \text{s.t.} \quad \phi_\theta(x) \geq 0, \quad \min_{u \in \mathcal{U}} \dot{\phi}_\theta(x, u) < -\eta. \quad (4)$$

The n^{th} -order safety index, ϕ_n , is parameterized by θ and is referred to as ϕ_θ . For clarity, ϕ_n and ϕ_θ are used interchangeably in this work. Given the problem's complexity, the method introduced by [12] is employed. This method leverages Positivstellensatz [28] to transform Problem 1 into a SOSP problem, which is then further converted into a nonlinear programming (NP) problem. Specifically, a refute set is constructed and proved empty by solving the SOSP, with detailed procedures outlined in [11]. The SOSP finds real-valued coefficients $q_i \in \mathbb{R}$, $p_i \geq 0, \forall i \in \mathbb{Z}_+$, such that

$$p_0 = -1 - \sum_{i=1}^{N_\zeta} q_i \zeta_i - p_1 \gamma_1 - p_2 \gamma_2 - \dots - p_N \gamma_N - p_{12} \gamma_1 \gamma_2 - \dots - p_{12\dots N} \gamma_1 \dots \gamma_N \in \text{SOS}. \quad (5)$$

where ζ_i, γ_i encompass the equality and inequality constraints in the SOS. Note that ζ_i and γ_i depend on the varying dynamics, including the varying parameters ρ . The feasible coefficients for (5) need to satisfy the positive semi-definite (PSD) decomposition $p_0 = \mathbf{x}^\top Q(\theta, \mathbf{p}, \rho) \mathbf{x}$ where $Q(\theta, \mathbf{x}, \rho) \succeq 0$. Let $\mathbf{x} := [1, x[1], \dots, x[N_x], x[1]x[2], \dots, x[N_x]^d]^\top$ contain all monomials of x with order no higher than d , assuming that p_0 has degree $2d$, and $\mathbf{p} := [p'_1, \dots, p'_{N_\zeta}, p_1, p_2, \dots, p_{012\dots N}]^\top$ be the auxiliary decision variable. With this, we have the final Nonlinear Program (NP), which provides the solution to Problem 1:

Problem 2. (Nonlinear Programming). *Find $\theta \in \Theta$ and \mathbf{p} where $\mathbf{p}[j] \in \mathbb{R}$ for $j > 0$ and $\mathbf{p}[j] \geq 0$ for $j > N_\zeta$, such that $Q(\theta, \mathbf{p}, \rho) \succeq 0$.*

The PSD condition can be verified through eigenvalue decomposition or by applying Sylvester's criterion to the determinants [29]. We utilize the eigenvalue decomposition in SIS and use Sylvester's criterion for SIA, to be introduced in the following subsection.

C. Safety Index Adaptation via DGA

SIA, a novel approach to solving Problem 1 introduced in [9], can efficiently adapt safety index parameter θ when the dynamics change, i.e., ρ changes to ρ' . Instead of performing the entire synthesis process again, SIA searches for a new point $(\theta', \mathbf{p}', \rho')$ in the neighborhood of the previous solution to Problem 2, $(\theta^*, \mathbf{p}^*, \rho)$, under the assumption that the change in ρ is bounded, i.e., $\|\rho - \rho'\| \leq \delta$ for some $\delta > 0$. Mathematically, this is formulated as:

Problem 3. (Safety Index Adaptation). *Find $\phi_{\theta'}$ that solves Problem 1 with system parameter ρ' given an originally feasible safety index ϕ_{θ^*} , i.e., $Q(\theta^*, \mathbf{p}^*, \rho) \succeq 0$.*

$$\theta', \mathbf{p}' = \arg \min_{\theta, \mathbf{p}} \mathcal{J}(\theta, \mathbf{p}) \text{ s.t. } Q(\theta, \mathbf{p}, \rho') \succeq 0. \quad (6)$$

In SIA, the constraint in (6) is satisfied via determinant gradient ascent (DGA). Sylvester's criterion [29] states that a Hermitian matrix is PSD if and only if all the principal minors are nonnegative. Then, the constraint in (6) is equivalent to

$$\text{Det}[Q(\theta, \mathbf{p}, \rho')]_{I,I} > 0, \quad \forall I \subseteq [1, \dots, M] \quad (7)$$

where M represents the size of Q and $[Q]_{I,I}$ denotes the submatrix of Q formed by selecting the rows indexed by I and columns indexed by J . Given that the principal minors are explicit functions of θ and \mathbf{p} , (7) can be satisfied via gradient ascends on these parameters with step size λ :

$$[\theta, \mathbf{p}] = [\theta, \mathbf{p}] + \lambda \delta \quad (8)$$

$$\delta = \nabla_{[\theta, \mathbf{p}]} \text{Det}[Q(\theta, \mathbf{p}, \rho')]_{I^*, I^*} \Big|_{\theta=\theta, \mathbf{p}=\mathbf{p}} \quad (9)$$

where $\text{Det}[Q(\theta, \mathbf{p}, \rho')]_{I^*, I^*}$ is the current lowest principal minor with indices I^* . SIA via DGA is significantly more time-efficient than the full synthesis and guarantees FI and FTC for \mathcal{X}_S^* with the updated $\phi_{\theta'}$ [9].

IV. PROBLEM FORMULATION

The system dynamics of the quadruped change with the package weight it carries. We first synthesize an initial safety index for the quadruped dynamics without payload. Then, SIA adapts this safety index for varying payloads. To effectively abstract out the complex dynamics and apply the adaptive safe control, we introduce the extended unicycle model and derive the SIS and SIA for the system in this section.

A. Extended Unicycle Dynamics

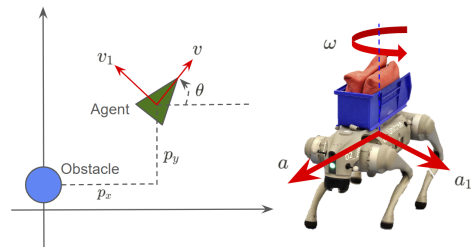


Fig. 2. The extended unicycle system models the Go2 quadruped in 2D and allows lateral movements on top of the classical unicycle dynamics.

For the quadruped dynamics, we follow the parameter-varying dynamic system (1). We introduce the extended unicycle system (Fig. 2), which extends the unicycle system with a quadruped's lateral movements, with states $x = [p_x, p_y, v, v_l, \theta]^\top$ and inputs $u = [a, a_l, \omega]^\top$.

$$f(x) = \begin{bmatrix} v \cdot \cos \theta - v_l \cdot \sin \theta \\ v \cdot \sin \theta + v_l \cdot \cos \theta \\ 0 \\ 0 \\ 0 \end{bmatrix}, g(x) = \begin{bmatrix} 0 & 0 & 0 \\ 0 & 0 & 0 \\ 1 & 0 & 0 \\ 0 & 1 & 0 \\ 0 & 0 & 1 \end{bmatrix} \quad (10)$$

where $p_x, p_y \in [-1, 1]$ m are the relative positions to the obstacle in the global frame, $v \in [-1.3, 1.3]$ m/s is the longitudinal body velocity, $v_l \in [-0.7, 0.7]$ m/s is the lateral body velocity, and θ is the yaw angle in the global frame. $a, a_l \in [-15, 15]$ m/s² are the longitudinal and lateral body acceleration commands and $\omega \in [-2, 2]$ rad/s is the yaw rate command. We set $A^f = \mathbf{I}_{5 \times 5}$, while A^g and ϵ take the following form:

$$A^g = \begin{bmatrix} 1 & 0 & 0 & 0 & 0 \\ 0 & 1 & 0 & 0 & 0 \\ 0 & 0 & \rho_{33}^g & \rho_{34}^g & \rho_{35}^g \\ 0 & 0 & \rho_{43}^g & \rho_{44}^g & \rho_{45}^g \\ 0 & 0 & \rho_{53}^g & \rho_{54}^g & \rho_{55}^g \end{bmatrix}, \epsilon = \begin{bmatrix} 0 \\ 0 \\ \rho_3^\epsilon \\ \rho_4^\epsilon \\ \rho_5^\epsilon \end{bmatrix}. \quad (11)$$

The varying parameters are identified prior to safety index synthesis and adaptation (Sec.V-B). (10) and (11) together form the parameter-varying dynamics (1).

B. SIS and SIA for Varying Quadruped Dynamics

We first derive the full SIS solution for the varying quadruped dynamics. We assume that the obstacle is at the origin and the safety specification is $\phi_0 = d_{\min}^2 - d^2$ where $d = \sqrt{p_x^2 + p_y^2}$, $d_{\min} = 1$ m. Then SIS produces a safety

index $\phi_\theta = \phi_0 + k\dot{\phi}_0$ such that the control law keeps the quadruped's center of mass at least d_{\min} distance away from the obstacle:

$$\phi_\theta = d_{\min}^2 - d^2 - 2kdd. \quad (12)$$

Here, we have a single safety index parameter $k \geq 0$. Taking the derivative of ϕ_θ , we get the main condition $\min_{u \in \mathcal{U}} \dot{\phi}_\theta(x, u) < -\eta$ as below

$$\begin{aligned} & -2kv^2 - 2kv_l^2 - 2p_x\alpha_1 - 2p_y\alpha_2 \\ & -2ka(-\alpha_3(\rho_{43}^g + \rho_{53}^g v) + \alpha_4(\rho_{33}^g - \rho_{53}^g v_l)) \\ & -2ka_l(-\alpha_3(\rho_{44}^g + \rho_{54}^g v) + \alpha_4(\rho_{34}^g - \rho_{54}^g v_l)) \\ & -2k\omega(-\alpha_3(\rho_{45}^g + \rho_{55}^g v) + \alpha_4(\rho_{35}^g - \rho_{55}^g v_l)) < -\eta \end{aligned} \quad (13)$$

where $\alpha_i, i = 1, 2, 3, 4$ encapsulate the trigonometric terms: $\alpha_1 = \cos \theta(k\rho_3^\epsilon + v - k\rho_5^\epsilon v_l) - \sin \theta(k\rho_4^\epsilon + v_l + k\rho_5^\epsilon v)$, $\alpha_2 = \cos \theta(k\rho_4^\epsilon + v_l + k\rho_5^\epsilon v) + \sin \theta(k\rho_3^\epsilon + v - k\rho_5^\epsilon v_l)$, $\alpha_3 = p_x \sin \theta - p_y \cos \theta$, $\alpha_4 = p_x \cos \theta + p_y \sin \theta$.

Since $k \geq 0$, the minimum of $\dot{\phi}_\theta$ is achieved at $a = a_{\max}$ if $-\alpha_3(\rho_{43}^g + \rho_{53}^g v) + \alpha_4(\rho_{33}^g - \rho_{53}^g v_l) \geq 0$ and $a = a_{\min}$ otherwise. Similarly, maximum and minimum control inputs are applied to a_l and ω based on the respective conditions. Using indicators $\mathbb{I}_{a, a_l, \omega} = \pm 1$, we can denote these conditions as

$$\mathbb{I}_a(-\alpha_3(\rho_{43}^g + \rho_{53}^g v) + \alpha_4(\rho_{33}^g - \rho_{53}^g v_l)) \geq 0 \quad (14)$$

$$\mathbb{I}_{a_l}(-\alpha_3(\rho_{44}^g + \rho_{54}^g v) + \alpha_4(\rho_{34}^g - \rho_{54}^g v_l)) \geq 0 \quad (15)$$

$$\mathbb{I}_\omega(-\alpha_3(\rho_{45}^g + \rho_{55}^g v) + \alpha_4(\rho_{35}^g - \rho_{55}^g v_l)) \geq 0. \quad (16)$$

In the main feasibility condition (13), we replace a with \tilde{a} , a_l with \tilde{a}_l , and ω with $\tilde{\omega}$. We have $\tilde{a} = a_{\max}$ if $\mathbb{I}_a = 1$ and $\tilde{a} = a_{\min}$ if $\mathbb{I}_a = -1$. Using the same rule, we set the values for \tilde{a}_l and $\tilde{\omega}$. We then add conditions for α_i 's and limits on states:

$$-\alpha_1^2 + (k\rho_3^\epsilon + v - k\rho_5^\epsilon v_l)^2 + (k\rho_4^\epsilon + v_l + k\rho_5^\epsilon v)^2 \geq 0 \quad (17)$$

$$-\alpha_2^2 + (k\rho_4^\epsilon + v_l + k\rho_5^\epsilon v)^2 + (k\rho_3^\epsilon + v - k\rho_5^\epsilon v_l)^2 \geq 0 \quad (18)$$

$$-\alpha_3^2 + p_x^2 + p_y^2 \geq 0 \quad (19)$$

$$-\alpha_4^2 + p_x^2 + p_y^2 \geq 0 \quad (20)$$

$$-p_x^2 + L^2 \geq 0 \quad (21)$$

$$-p_y^2 + L^2 \geq 0 \quad (22)$$

$$-v^2 + V^2 \geq 0 \quad (23)$$

$$-v_l^2 + V_l^2 \geq 0 \quad (24)$$

$$p_x^2 + p_y^2 - d_{\min}^2 \geq 0 \quad (25)$$

where $L = 1\text{m}$, $V = 1.3\text{m/s}$, and $V_l = 0.7\text{m/s}$ are identified as reasonable limits for the states during the system identification procedure (Sec. V-B).

We omit the last condition in (4), $\phi_\theta \geq 0$, to allow the safety index to decrease at all levels, i.e., $\phi_\theta \in \mathbb{R}$, with $\eta = 1e-6$. With these, we construct a refute set by negating (13) and gathering (14)~(25), and prove that this refute set is empty. This is equivalent to solving Problem 1 [11]. There are 8 versions of the refute set, each assigned with different sign values of $\mathbb{I}_{a, a_l, \omega}$. The i^{th} assignment ($i \in [8]$) of $(\mathbb{I}_a, \mathbb{I}_{a_l}, \mathbb{I}_\omega)$ leads to the following SOSP problem based on (5):

$$p_{i,0} = \mathbf{x}^\top Q_i(\theta, \mathbf{p}_i, \rho) \mathbf{x} = -1 - \sum_{n=1}^{13} p_{i,n} \gamma_{i,n} \quad (26)$$

where $\mathbf{x} := [1, \alpha_1, \alpha_2, \alpha_3, \alpha_4, p_x, p_y, v, v_l]^\top$, $\theta := [k]$, $\mathbf{p}_i := [p_{i,1}, \dots, p_{i,13}]$, $\rho := [\rho_{33}^g, \rho_{34}^g, \dots, \rho_{55}^g, \rho_3^\epsilon, \rho_4^\epsilon, \rho_5^\epsilon]$, and $\gamma_{i,n}$, $i \in [1:13]$ encodes inequality constraints (13)~(25).

Once the varying parameters change to ρ' , the derivatives of the principal minors of $\{Q_i\}_{i=1,\dots,8}$ with respect to $[\theta, \mathbf{p}_1, \dots, \mathbf{p}_8]$ are computed to apply (8):

$$\delta_\theta = \frac{1}{8} \sum_{i=1}^8 \nabla_\theta \text{Det}[Q_i(\theta, \mathbf{p}_i, \rho')]_{I_i^*, I_i^*} \Big|_{\theta=\theta, \mathbf{p}_i=\mathbf{p}_i} \quad (27)$$

$$\delta_{\mathbf{p}_i} = \nabla_{\mathbf{p}_i} \text{Det}[Q_i(\theta, \mathbf{p}_i, \rho')]_{I_i^*, I_i^*} \Big|_{\theta=\theta, \mathbf{p}_i=\mathbf{p}_i}. \quad (28)$$

We apply the following update rules

$$\theta = \theta + \lambda_\theta \delta_\theta, \quad \mathbf{p}_i = \mathbf{p}_i + \lambda_{\mathbf{p}} \delta_{\mathbf{p}_i} \quad (29)$$

with learning rates $\lambda_{\theta, \mathbf{p}} = 1e-3$ and a discount factor of 0.99 until all principal minors of all Q_i 's are below a set target value. Once this is achieved, the safety index parameter θ is adapted to the new parameters ρ' .

Remark. Although gradient updates with a pre-computed symbolic expression of Q are efficient for low-dimensional systems [9], the size of our Q matrix makes this approach inefficient. Therefore, we utilize finite-differentiation in place of symbolic gradient updates. Both methods yield nearly identical solutions, as the search is limited to a local space.

V. HARDWARE SETUP AND SYSTEM IDENTIFICATION

Naturally, the first step in safety index adaptation is identifying the varying parameters for different payloads, enabling DGA. We use payloads of 0.0kg (empty basket), 3.5kg, and 5.9kg. This section details the hardware, system identification process, and the identified varying parameters.

A. Unitree Go2 Quadruped

The Unitree Go2 quadruped (Fig. 2) is controlled with high-level velocity commands in the body frame. To translate the acceleration commands in the extended unicycle dynamics (1) to velocity commands used by the hardware interface, we perform numerical integration of the acceleration commands:

$$\mathbf{v}_{cmd} = \mathbf{v}_{meas} + \mathbf{a}_{cmd} dt, \quad (30)$$

where $dt = 1/30\text{Hz}$ is the control period. While the Go2 is controlled with high-level commands, the low-level controller is left unaltered. Inevitably, the low-level controller interferes with the high-level commands to rebalance the quadruped. However, when the commands lead to an unsalvageable state, the quadruped falls down.

B. System Identification for Varying Parameters

To excite the system, high-level body velocity and yaw rate commands $u_{sid} = [v^{sid}, v_l^{sid}, \omega^{sid}]$ are generated as sinusoidal waves with various frequencies and amplitudes of 1m/s, 0.3m/s, 1.75rad/s, for each command. An Optitrack system captures p_x, p_y, θ , while Go2 sensors measure body velocities v, v_l, θ . For data-processing, we convert body velocity commands to desired accelerations by reversing (30).

System data is collected for each payload, and smoothed using a LOWESS (Locally Weighted Scatterplot Smoothing) filter. In the data we collected, the quadruped's velocities exceed the specified sinusoidal command amplitudes due to the added weights. Thus, we set state limits for SIS and SIA to be $v \in [-1.3, 1.3]$ m/s and $v_l \in [-0.7, 0.7]$ m/s. Using the filtered data, a least-squares regression is applied to fit A^g and ϵ for each package weight. The final varying parameter values are shown in Table I. The identified parameters result in an average coefficient of determination above 0.78.

TABLE I

VARYING PARAMETERS IDENTIFIED FROM SYSTEM IDENTIFICATION

Payload (kg)	A^g Values ($\rho_{i,j}^g, \forall i, j \in [3:5]$)			ϵ Values
0.0	0.08177	0.05700	-0.00152	-0.13288
	0.00742	0.12048	0.00241	0.23156
	-0.00166	0.00444	0.70741	0.01311
3.5	0.11144	0.02731	0.00278	-0.24451
	0.03285	0.13207	0.00682	0.10565
	-0.00121	0.00207	0.68546	0.01923
5.9	0.12088	0.00613	0.00498	-0.44301
	0.04936	0.10012	-0.03498	0.09005
	0.00031	-0.00129	0.66063	0.02785

VI. EXPERIMENTS

We first conduct a numerical study on safety indices produced by SIS and SIA for varying parameters across different packages. We then deploy the safety indices on a quadruped to validate their real-time performance. The quadruped, carrying different payloads, adapts its safety index and maneuvers around obstacles to reach target locations. Both numerical and hardware experiments reveal failure cases for the non-adapted safety index. Using SIA, the safety objectives are consistently met.

A. Numerical Study

We first solve the full SIS for the parameters identified for the 0.0kg payload, $\rho_{0,0}$, in MATLAB using `fmincon` as the solver. Then, we further refine the resulting parameters using the update rule (29) to achieve the desired safety guarantees for the 0.0kg payload dynamics. We suspect that the refute set and the number of parameters are too large for the full SIS to converge to an optimal solution before the solver terminates. The update rule (29) is effective in converging to a local optimum, refining the safety index to meet the desired safety guarantees. The final initial safety index is $\phi_{0,0}$. The update rule (29) is then applied for the 3.5kg payload parameters $\rho_{3,5}$ to adapt $\phi_{0,0}$ to $\phi_{3,5}$. Then, $\phi_{3,5}$ is adapted to the 5.9kg payload parameters $\rho_{5,9}$, producing the safety index $\phi_{5,9}$. As seen in Table II, SIA takes significantly less computation time to update the safety index, approximately 1.48% of the computation time for the full synthesis and refinement combined. Furthermore, we improve the computational efficiency of SIA by 96.5% using finite-differentiation instead of symbolic gradient computation.

TABLE II

SIS AND SIA COMPUTATION TIME AND SAFETY INDEX PARAMETERS

	$\phi_{0,0}$	$\phi_{3,5}$	$\phi_{5,9}$
k	0.61068	0.64608	0.67905
Finite-diff. Time (sec)	562.92	9.69	7.04
Symbolic-grad. Time (sec)	-	398.79	76.10

Note that the safety index parameter, k , increases with heavier payloads (Table II). As discussed in [9], a system is less sensitive to the inputs when the varying parameters decrease, and thus requires a more aggressive safe control law to react to unsafe regions in advance, i.e., higher k values. In Table I, observe that $\rho_{5,5}^g$ decreases as the payload gets heavier. Therefore, the increase in k values for heavier payloads is well-aligned with the previous findings.

We proceed with sampled-based feasibility experiments. The non-adapted safety index, $\phi_{0,0}$, and adapted safety indices, $\phi_{3,5}$ and $\phi_{5,9}$, are used to run the following safe control laws under different payload dynamics:

$$\min_{u \in \mathcal{U}} \mathcal{J}(u) \quad \text{s.t.} \quad \dot{\phi}_\theta(x, u) \leq 0 \quad \text{if} \quad \phi_\theta(x) < 0 \quad (31)$$

$$\min_{u \in \mathcal{U}} \mathcal{J}(u) \quad \text{s.t.} \quad \dot{\phi}_\theta(x, u) < -\eta \quad \text{if} \quad \phi_\theta(x) \geq 0 \quad (32)$$

If (31) is feasible, the safety index is FI feasible for that state. Similarly, if (32) is feasible, the safety index is FTC feasible. For each controller-dynamics pair (Table III), FI and FTC feasibilities are each evaluated for 1000 uniformly sampled states. All the safety indices achieve 100% feasibility for both FI and FTC in their matching dynamics, e.g., $\phi_{5,9}$ in 5.9kg dynamics. However, $\phi_{0,0}$ fails the FTC condition while the adapted safety indices maintain 100% feasibility in higher velocity states for 3.5kg and 5.9kg payloads dynamics.

TABLE III

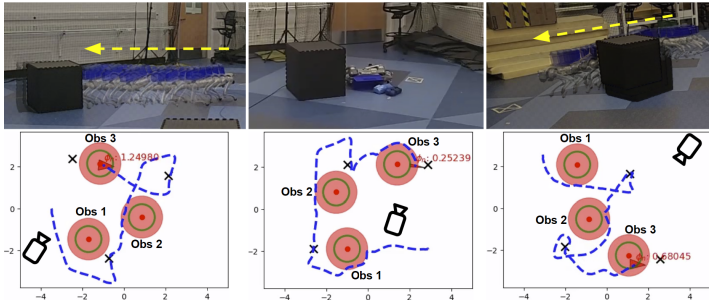
NON-ADAPTED VS. ADAPTED SAFETY INDEX FEASIBILITY

Dynamics Safety Index	Non-adapted Safety Index			Adapted Safety Index		
	$\rho_{0,0}$ $\phi_{0,0}$	$\rho_{3,5}$ $\phi_{0,0}$	$\rho_{5,9}$ $\phi_{0,0}$	$\rho_{3,5}$ $\phi_{3,5}$	$\rho_{5,9}$ $\phi_{3,5}$	$\rho_{5,9}$ $\phi_{5,9}$
FI (1000 states)	100%	100%	100%	100%	100%	100%
FTC (1000 states)	100%	99.8%	99.8%	100%	100%	100%

B. Package-carrying Quadruped Hardware Experiments

We validate SIA's effectiveness in a real-world scenario where the quadruped navigates through obstacles while carrying varying payloads. As shown in Fig. 1, the quadruped clears each obstacle and reaches the goal locations sequentially, starting with no payload (0.0kg) and loaded with 3.5kg and 5.9kg packages at the subsequent goals. The safety index considers only one obstacle at a time. The quadruped waits 5 seconds at each goal for package loading, synchronized with SIA computation time for realism. We use the non-adapted safety index $\phi_{0,0}$ as a baseline, while our method adapts the safety index, starting with $\phi_{0,0}$ and adjusting to $\phi_{3,5}$ and $\phi_{5,9}$ as dynamics change. Note that SIA is done offline and we implement a switch mechanism to update the safety index.

We use three distinct goal-obstacle courses, each repeated multiple times for consistency. The varying goal and obstacle positions, shown in the bottom row of Fig. 3, require the quadruped to avoid obstacles from different directions. For instance, in Course 1, it moves forward to the second obstacle and backward to the third, while in Course 3, it moves backward to the second and forward to the third. This variation allows us to evaluate the effectiveness of SIA in real-world scenarios thoroughly. LQR controller is used as the nominal controller and the safe control u is computed as



follows, converting (3) into a quadratic program (QP) [13]: when $\phi_\theta \geq 0$, $u = \arg \min_{u \in \mathcal{U}} \|u - u_{\text{nom}}\|_2^2$ s.t. $\dot{\phi}_\theta < -\eta$.

TABLE IV
QUADRUPED HARDWARE EXPERIMENT RESULT

Obstacle Course	Non-adapted Safety Index Success % (Success/Trial)	Adapted Safety Index Success % (Success/Trial)
Course 1	80% (4/5)	100% (10/10)
Course 2	60% (3/5)	100% (6/6)
Course 3	80% (4/5)	100% (7/7)

Table IV shows that the adapted safety indices achieve 100% safety, ensuring the quadruped avoids all obstacles without losing balance. In contrast, the non-adapted safety index fails to satisfy the safety guarantees across all three courses when carrying the 5.9kg package (Fig. 3). In Course 1, the QP fails when the quadruped nears its velocity limit ($v = -1.14\text{m/s}$), causing a collision as it moves directly toward the obstacle in reverse. In Course 2, the quadruped loses balance and falls while trying to track an overly aggressive control input in an unsafe region. In Course 3, the non-adapted safety index does not provide sufficient control input to ensure prompt FTC, leading to another collision.

C. Discussion

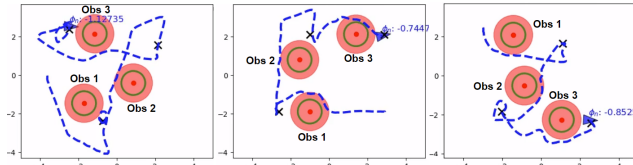


Fig. 4. Full trajectories using SIA in Courses 1, 2, and 3.

In this work, we deploy a continuous-time (CT) safe control law in a discrete-time (DT) real system. SSA offers a modified DT safe control law that accounts for discretization errors [30], by incorporating a safety margin $\sigma \in \mathbb{R}_+$ in the safety index formulation: $\phi_\theta = \sigma + d_{\min}^2 - d^2 - 2kdd$. Without this margin, the adapted safety indices enter the unsafe set \mathcal{X}_S^C , illustrated as light red circles in Fig. 4, violating the FI guarantee in practice. To examine whether the deployed safety indices would violate the FI guarantee with a DT safety margin, we derive the practical margin from our hardware experiments: $\sigma_{\text{DT}} = \Delta d_{\max}^2 + 2\Delta d_{\max} \cdot d_{\min}$, where $\Delta d_{\max} = 0.375\text{m}$ is the largest change in quadruped position over one timestep. Adding σ_{DT} indicates that the radius of the unsafe set is padded with Δd_{\max} . We account

for the discretization error by padding the safety index with this value (shown with green solid lines in Fig. 3 and Fig. 4). With σ_{DT} , we see that the adapted safety indices never enter the padded unsafe sets (Fig. 4), indicating that the FI is guaranteed, while the non-adapted safety index still violates the FI guarantee (Fig. 3).

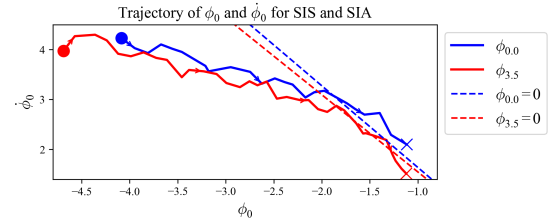


Fig. 5. Trajectories (solid lines) of ϕ_0 and $\dot{\phi}_0$ for the non-adapted and adapted safety indices from hardware deployment. The segments move from solid circles to crossmarks. Blue lines are for the non-adapted case and the red lines are for the adapted case. Dashed lines denote the CT safe set boundaries.

In (12), observe that a larger k value forces the safe control law to be more pre-emptive, e.g., when the quadruped is approaching an obstacle at high speed, a larger k value triggers the $\phi_\theta \geq 0$ condition in (3) earlier than a lower k value would. In Fig. 5, notice that the red solid line ($\phi_{3.5}$ with $k = 0.64608$) starts moving away from CT boundary earlier and faster than the blue solid line ($\phi_{0.0}$ with $k = 0.61068$). Although $\phi_{3.5}$ also invades the CT boundary, its magnitude is much smaller than $\phi_{0.0}$ and it converges back into the safe region much faster. This allows the adapted safety index to shift away from unsafe regions earlier and faster, illustrating how SIA adapts the safety index to the varying dynamics.

VII. CONCLUSION AND FUTURE WORK

In this paper, we improve the efficiency of SIA and demonstrate its ability to guarantee safety for quadruped robots in varying dynamics. We also analyze the DT safety margin and its impact, demonstrating that SIA guarantees FI with the margin, while non-adapted cases still fail. We plan to synthesize and adapt a DT safety index for deployment in future work. Additionally, we aim to incorporate an online estimator for the varying parameters.

ACKNOWLEDGEMENT

The authors would like to thank Weiye Zhao at Carnegie Mellon University for technical guidance. Chase Dunaway is supported by the National Science Foundation (NSF) under Grant No. 1950811.

REFERENCES

- [1] A. Xiao, W. Tong, L. Yang, J. Zeng, Z. Li, and K. Sreenath. “Robotic Guide Dog: Leading a Human with Leash-Guided Hybrid Physical Interaction”. In: *International Conference on Robotics and Automation*. 2021.
- [2] C. Yang, G. N. Sue, Z. Li, L. Yang, H. Shen, Y. Chi, A. Rai, J. Zeng, and K. Sreenath. “Collaborative Navigation and Manipulation of a Cable-Towed Load by Multiple Quadrupedal Robots”. In: *IEEE Robotics and Automation Letters*. 2022.
- [3] X. Cheng, K. Shi, A. Agarwal, and D. Pathak. “Extreme Parkour with Legged Robots”. In: *IEEE International Conference on Robotics and Automation*. 2024.
- [4] R. Liu, R. Chen, and C. Liu. “Safe Interactive Industrial Robots using Jerk-based Safe Set Algorithm”. In: *International Symposium on Flexible Automation*. 2022.
- [5] H.-C. Lin, C. Liu, Y. Fan, and M. Tomizuka. “Real-time collision avoidance algorithm on industrial manipulators”. In: *Conference on Control Technology and Applications*. 2017.
- [6] T. He, C. Zhang, W. Xiao, G. He, C. Liu, and G. Shi. “Agile But Safe: Learning Collision-Free High-Speed Legged Locomotion”. In: *Robotics: Science and Systems (RSS)*. 2024.
- [7] R. Liu, Y. Sun, and C. Liu. “Robotic LEGO Assembly and Disassembly from Human Demonstration”. In: *International Symposium on Flexible Automation*. 2024.
- [8] A. Shek, B. Y. Su, R. Chen, and C. Liu. “Learning from Physical Human Feedback: An Object-Centric One-Shot Adaptation Method”. In: *International Conference on Robotics and Automation*. 2023.
- [9] R. Chen, W. Zhao, R. Liu, W. Zhang, and C. Liu. “Real-time Safety Index Adaptation for Parameter-varying Systems via Determinant Gradient Ascend”. In: *American Control Conference*. 2024.
- [10] C. Liu and M. Tomizuka. “Control in a safe set: Addressing safety in human-robot interactions”. In: *Dynamic Systems and Control Conference*. 2014.
- [11] R. Chen, W. Zhao, and C. Liu. “Safety Index Synthesis with State-dependent Control Space”. In: *American Controls Conference*. 2024.
- [12] W. Zhao, T. He, T. Wei, S. Liu, and C. Liu. “Safety Index Synthesis via Sum-of-Squares Programming”. In: *American Control Conference*. 2023.
- [13] A. D. Ames, J. W. Grizzle, and P. Tabuada. “Control barrier function based quadratic programs with application to adaptive cruise control”. In: *Conference on Decision and Control*. 2014.
- [14] A. D. Ames, S. Coogan, M. Egerstedt, G. Notomista, K. Sreenath, and P. Tabuada. “Control barrier functions: Theory and applications”. In: *European control conference*. 2019.
- [15] A. Clark. “A Semi-Algebraic Framework for Verification and Synthesis of Control Barrier Functions”. In: (2024). arXiv: 2209.00081 [eess.SY].
- [16] H. Dai and F. Permenter. “Convex synthesis and verification of control-Lyapunov and barrier functions with input constraints”. In: *American Control Conference*. 2023.
- [17] S. Kang, Y. Chen, H. Yang, and M. Pavone. “Verification and synthesis of robust control barrier functions: Multilevel polynomial optimization and semidefinite relaxation”. In: *Conference on Decision and Control*. 2023.
- [18] S. Liu, J. Dolan, and C. Liu. “Safe control under input saturation with neural control barrier functions”. In: *Conference on Robot Learning*. 2022.
- [19] C. Dawson, S. Gao, and C. Fan. “Safe Control With Learned Certificates: A Survey of Neural Lyapunov, Barrier, and Contraction Methods for Robotics and Control”. In: *IEEE Transactions on Robotics* (2023).
- [20] X. Xu, P. Tabuada, J. W. Grizzle, and A. D. Ames. “Robustness of control barrier functions for safety critical control”. In: *IFAC-PapersOnLine* 48.27 (2015), pp. 54–61.
- [21] M. Jankovic. “Robust control barrier functions for constrained stabilization of nonlinear systems”. In: *Automatica* 96 (2018), pp. 359–367.
- [22] A. J. Taylor and A. D. Ames. “Adaptive safety with control barrier functions”. In: *American Control Conference*. 2020.
- [23] S. Liu, K. S. Yun, J. M. Dolan, and C. Liu. “Synthesis and Verification of Robust-Adaptive Safe Controllers”. In: *European Control Conference*. 2024.
- [24] D. D. Fan, J. Nguyen, R. Thakker, N. Alatur, A.-a. Aghamohammadi, and E. A. Theodorou. “Bayesian Learning-Based Adaptive Control for Safety Critical Systems”. In: *International Conference on Robotics and Automation*. 2020.
- [25] L. Brunke, S. Zhou, and A. P. Schoellig. “Barrier Bayesian Linear Regression: Online Learning of Control Barrier Conditions for Safety-Critical Control of Uncertain Systems”. In: *Annual Learning for Dynamics and Control Conference*. 2022.
- [26] R. Grandia, A. J. Taylor, A. D. Ames, and M. Hutter. “Multi-Layered Safety for Legged Robots via Control Barrier Functions and Model Predictive Control”. In: *International Conference on Robotics and Automation*. 2021.
- [27] Q. Liao, Z. Li, A. Thirugnanam, J. Zeng, and K. Sreenath. “Walking in Narrow Spaces: Safety-Critical Locomotion Control for Quadrupedal Robots with Duality-Based Optimization”. In: *International Conference on Intelligent Robots and Systems*. 2023.
- [28] P. A. Parrilo. “Semidefinite programming relaxations for semialgebraic problems”. In: *Mathematical programming* 96 (2003), pp. 293–320.
- [29] R. A. Horn and C. R. Johnson. *Matrix analysis*. Cambridge university press, 2012.
- [30] W. Zhao, T. He, F. Li, and C. Liu. “Implicit Safe Set Algorithm for Provably Safe Reinforcement Learning”. In: 2024. arXiv: 2405.02754 [cs.RO].